Materials Science & Engineering A 668 (2016) 263–270

Contents lists available at ScienceDirect

Materials Science & Engineering A

journal homepage: www.elsevier.com/locate/msea

The effects of thermomechanical history on the microstructure of a nickel-base superalloy during forging

S. Gardner [a,*], W. Li [b], M. Coleman [a], R. Johnston [a,*]

[a] College of Engineering, Bay Campus, Swansea University, Swansea SA1 8EN, UK
[b] Rolls-Royce plc, PO Box 31, Derby DE24 8BJ, UK

ARTICLE INFO

Article history:
Received 14 March 2016
Received in revised form
13 May 2016
Accepted 14 May 2016
Available online 16 May 2016

Keywords:
HAYNES® 282®
Interrupted hot compression
Grain growth
Recrystallization
Annealing

ABSTRACT

The effect of thermo-mechanical history on hot compression behaviour and resulting microstructures of a nickel base superalloy is presented. Hot compression tests were carried out on HAYNES® 282® specimens to varying strains from 0.1 to 0.8. Both single pass and multi-pass tests were completed. 60 min inter-pass times were utilized to accurately replicate industrial forging practices. The effect of dynamic, metadynamic and static recrystallization during inter-pass times on flow stress was investigated. The resulting microstructures were analysed using scanning electron, optical microscopy and EBSD to relate grain size and homogeneity with flow stress data. The study showed a negligible difference between multi-pass and single pass tests for strain increments above 0.2. Therefore, when modelling similar low strain and strain rate forging processes in HAYNES® 282®, previous forging steps can be ignored.

1. Introduction

Casings are key structural components in a gas turbine engine. They are designed to contain the gas stream, provide housing for the various hot section components, and provide containment in the event of a mechanical failure. Nickel-based superalloys are able to withstand the high temperatures experienced in the combustor and turbine sections. Typically, casings are manufactured by multiple forging operations which include: upsetting, punching, piercing, becking, and ring rolling. Ring rolling is a low strain rate operation typically completed in multiple steps, requiring reheats in-between to bring the material back up to a workable temperature. By altering various forging and heat treatment parameters, the final microstructure and mechanical properties of the component can be tailored to specific requirements. To save materials, costs and time, FE models are typically used to predict microstructural evolution during a single forging processes [1]. However due to the multi-pass forging route employed during the manufacture of casings, it is unknown whether modelling the final stage of a forging route will yield accurate results, or whether the thermomechanical history of the material needs to be taken into account.

Attempts have been made to model the various ring rolling parameters and therefore predict the final microstructure and mechanical properties of a finished component. An early study [2] developed a coupled thermomechanical model incorporating heat transfer. Recently studies have utilized finite element software DEFORM 3D [3] to model the ring rolling process. Previous studies investigated the effect of processing parameters on recrystallization and final grain size, although these studies did not take into account previous thermomechanical history [4,5]. Previous work has investigated the effect of prior deformation steps and final annealing on microstructure evolution though interrupted hot compression studies. These studies looked into varying strain, and different materials such as magnesium [6], steel [7] and nickel [8]. These studies concluded that there was a difference between single-pass and multi-pass microstructures. Orientation has been shown to effect recrystallization rates in multi-hot experiments [9]. However these studies all utilized short inter-pass times, focusing on metadynamic rather than static recrystallization – therefore not representative of the industrial practice for a ring rolling route. Slightly longer inter-pass times were used in an investigation into magnesium, which showed flow hardening occurring during the inter-pass anneal [10]. Multi-pass flow stress behaviour in Aluminium has also been predicted in recent work [11]. Recently a study has shown that the final grain size of HAYNES® 282® is primarily dependent on annealing time and temperature, not forging strain and strain rate. However this study only considered a single-step process [12].

The aim of this experiment is to investigate the effect of thermomechanical history on final microstructure through a series of

* Corresponding authors.
E-mail addresses: 485354@swansea.ac.uk (S. Gardner), r.johnston@swansea.ac.uk (R. Johnston).

http://dx.doi.org/10.1016/j.msea.2016.05.051

interrupted hot compression experiments. In particular, comparing the differences, if any, between single and multi-pass compression tests and whether this is dependent on strain. The results will determine whether thermomechanical history should be taken into account when replicating forging conditions in both a laboratory environment and within a model.

2. Materials and methods

The material used for this investigation was HAYNES® 282®an age-hardenable gamma-prime-strengthened nickel-based superalloy. The composition for Haynes 282 is shown in Table 1 [13]. The material was supplied in the form of a 100 mm diameter billet that was 80 mm high and approximately 5 kg in weight. 14 cylindrical specimens (8 mm diameter, 12 mm height) were sectioned from the billet using wire electric discharge machining (EDM).

The initial microstructure was typical of an annealed billet product with a grain size of approximately 75 μm, shown in Fig. 1.

Compression testing was completed on a uniaxial hydraulic compression rig with a split furnace capable of 1200 °C. Tests complied with ASTM E209-00(2010) and were performed under stroke control. Specimens underwent a 3 min soak time at 1100 °C prior to the start of the test to equalise temperatures within the specimen and furnace. Boron nitride spray was used as a lubricant between the specimen faces in contact with the loading platens. Post-test specimens were removed immediately and left to air cool; replicating industrial practice. Multistage tests underwent a 1 h dwell at 1100 °C between compression stages. In total 14 tests were conducted at 1100 °C at a strain rate of 0.2/s. Specimens were deformed to compressive strains of 0.6, 0.8 and 0.1. Additionally, multistage tests were deformed by compressive strains of 3×0.2 and $0.7+0.1$. The test conditions aim to replicate the typical strains, strain rates, and temperatures experienced during a complete ring rolling process. The conditions were extracted from a FE DEFORM-3D V.11 [3] ring rolling model replicating observed typical industrial processing parameters for nickel-based superalloys. Seven specimens underwent a direct age heat treatment, which consisted of 2 h soak at 1010 °C then air cooled, followed by an 8 h soak at 788 °C then air cooled.

Specimens were mounted in conductive bakelite and polished to a 1 μm diamond lubricant finish before being etched with Kallings II [14] to reveal the grain boundaries. Images were captured using an optical light microscope and analysed using the software ImageJ [15]. DEFORM models were used to generate a strain map of the specimen cross section, to accurately predict local strains and strain rates; correlating microstructures to local deformation conditions. Energy-dispersive X-ray spectroscopy (EDX) was conducted using a Phillips XL-30 scanning electron microscope (SEM). Electron back scatter diffraction (EBSD) analysis was conducted on the same instrument operated at 20 kV integrated to a Nordlys EBSD detector using HKL Technology Channel 5 software.

3. Results

3.1. Dynamic recrystallization rate

In order to establish the amount of dynamic recrystallization (DRX) which occurred during each deformation pass, it was necessary to predict the relationship between fraction of dynamically recrystallized grains and strain. The flow stress data was analysed from a single pass compression test to 0.6 strain. Using a model proposed by Estrin and Mecking [16] and adapted by Chen et al. [17] it is possible to predict the volume fraction of DRX grains

Table 1.
Composition of Haynes 282 wt%.

Ni	Cr	Co	Mo	Ti	Al	Fe	Mn	Si	C	B
57[a]	20	10	8.5	2.1	1.5	1.5[b]	0.3	0.15	0.06	0.005

[a] Nickel as balance.
[b] Maximum.

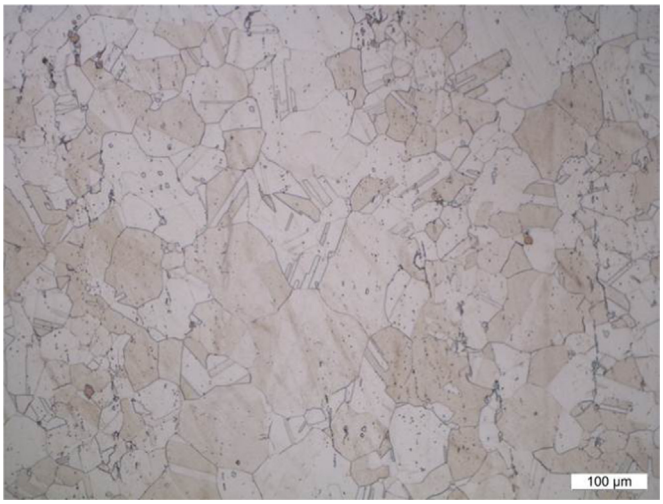

Fig. 1. The initial microstructure of the as received Haynes 282 billet showing a grain size of 75 μm.

(Eq. (1))

$$X = \frac{\sigma_{DRV} - \sigma}{\sigma_{sat} - \sigma_{ss}} \tag{1}$$

where X=fraction recrystallized, σ_{DRV}=theoretical flow stress in the absence of DRX, σ=observed flow stress, σ_{sat}=saturation flow stress, σ_{ss}=steady state flow stress. The theoretical flow stress in the absence of DRX is driven purely by work hardening and dynamic recovery (DRV), and can be calculated using Eq. (2).

$$\sigma_{DRV} = \sqrt{\sigma_{sat}^2 - (\sigma_{sat}^2 - \sigma_{crit}^2)\exp(-\Omega\varepsilon)} \tag{2}$$

σ_{sat}, σ_{ss} and critical strain (σ_{crit}) can be calculated by plotting work hardening rate ($\theta = d\sigma/d\varepsilon$) vs flow stress, as shown in Fig. 2. The critical stress for DRX under these conditions is 178 MPa, which corresponds to a critical true strain of 0.09.

The coefficient of dynamic recovery Ω is obtained using the linear regression method by plotting Eq. (3) as shown in Fig. 3.

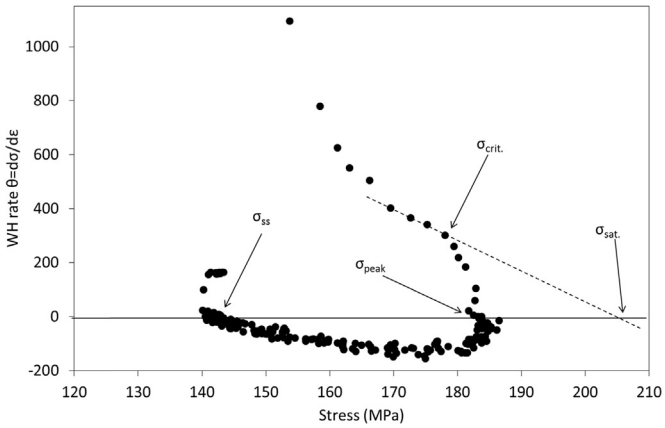

Fig. 2. Work hardening rate vs stress plot used to obtain key stresses.

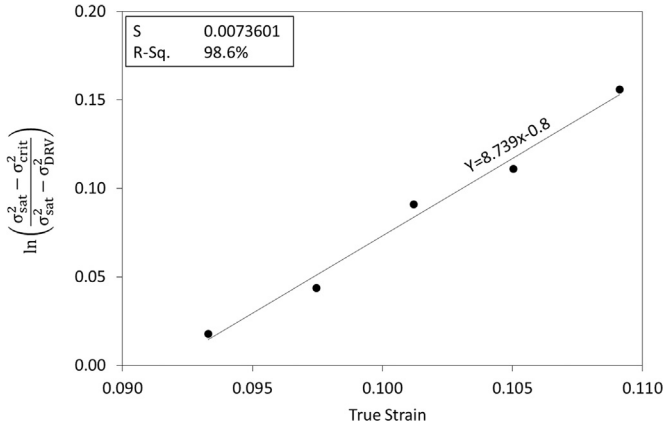

Fig. 3. Coefficient of dynamic recovery derived using the linear regression method.

$$\Omega e = ln\left(\frac{\sigma_{sat}^2 - \sigma_{crit}^2}{\sigma_{sat}^2 - \sigma_{DRV}^2}\right) \quad (3)$$

where σ_{DRV}^2 is the flow stress immediately prior to σ_{crit}^2.

Once Ω and the fundamental stresses have been obtained it is possible to plot the dynamic recrystallization fraction against strain as shown in Fig. 4. This recrystallization curve is only valid for 1100 °C and a strain rate of 0.2/s.

Fig. 4 indicates that the fraction recrystallized demonstrates a sigmoidal dependence on true strain. It can be determined that at a true strain of 0.2, approximately 10% of grains have recrystallized and 50% recrystallization is achieved at a true strain of 0.4. The microstructure is fully recrystallized at a true strain of 0.8.

3.2. Interrupted flow stress curves

Typical flow stress curves for single pass and multi-pass tests to 0.6 engineering strain are displayed in Fig. 5. The curves are a flow softening type where the flow stress work hardens to a peak strain then decreases as the material softens due to dynamic re-crystallization. For non-interrupted tests the material continues to soften before reaching steady state at a true strain of 0.8. For interrupted tests the curves show the material reaching a critical strain before beginning to soften. However due to the test being interrupted the softening is relatively minor and the final flow stress remains close to the maximum.

Unusually, it can be seen that after the inter-pass anneal, upon reloading, the flow stress for the 2nd and 3rd pass hardens and replicates the 1st stage instead of continuing to soften. Yield peaks are visible upon reloading for all interrupted compression tests. A

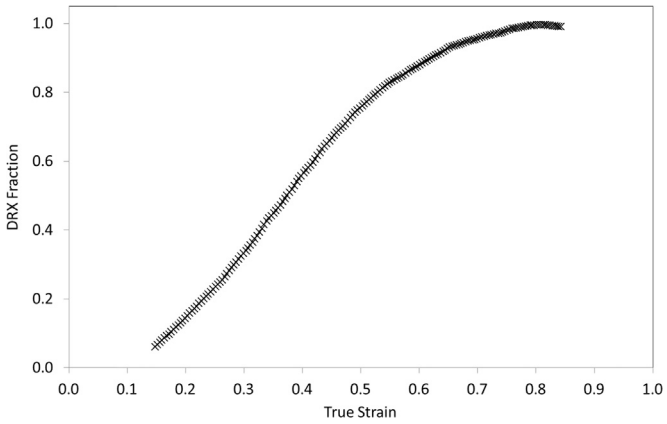

Fig. 4. Dynamic recrystallization volume fraction vs true strain.

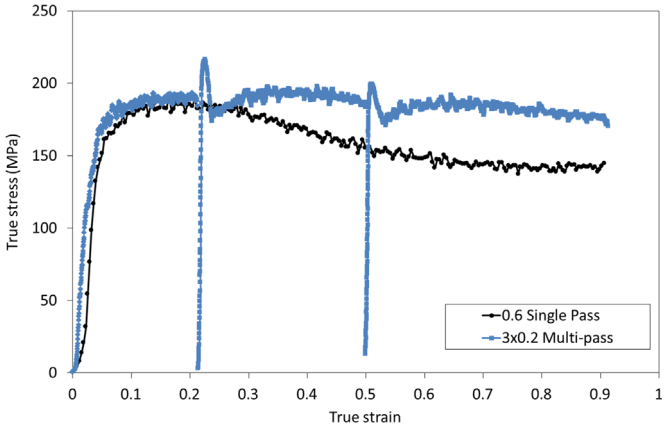

Fig. 5. An interrupted multi-pass test compared to a single pass test, showing the effect of a 1 h interpass dwell.

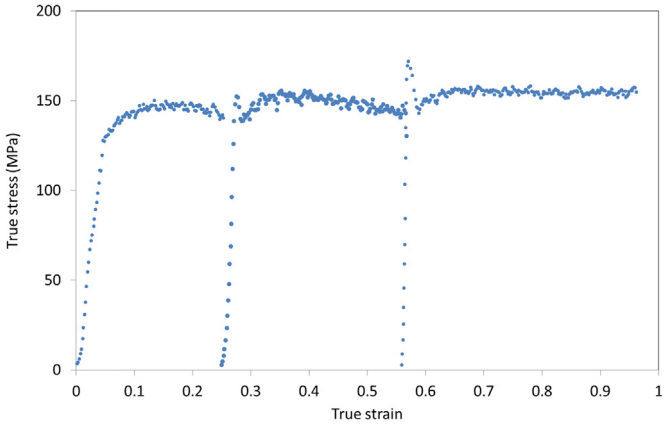

Fig. 6. Interrupted hot compression test at 1150 °C. The yield peaks are still visible at this temperature suggesting they could be caused by friction.

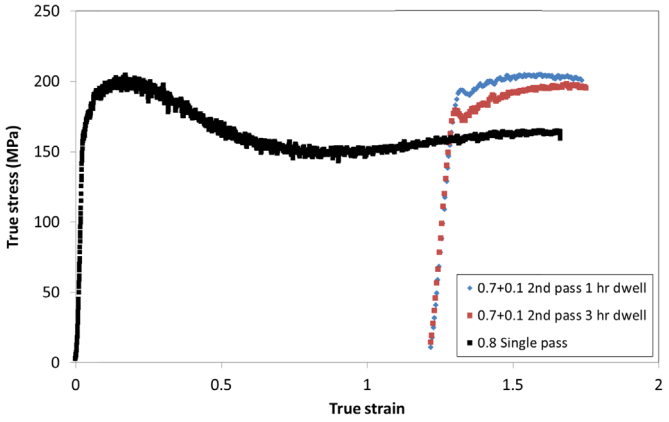

Fig. 7. Effect of a 1 h and 3 h dwell on high strain interrupted tests.

further test, shown in Fig. 6 was conducted at 1150 °C to investigate whether any solute atoms may be pinning the grain boundaries. The yield peaks were still visible at this higher temperature.

Fig. 7 displays a single and multi-pass test compressed to 0.8 engineering strain. A similar flow softening behaviour can be observed. As with the 0.6 engineering strain test, the flow stress appears to reach steady state at a true strain of 0.8, suggesting that full dynamic recrystallization has occurred. The 2nd pass follows a

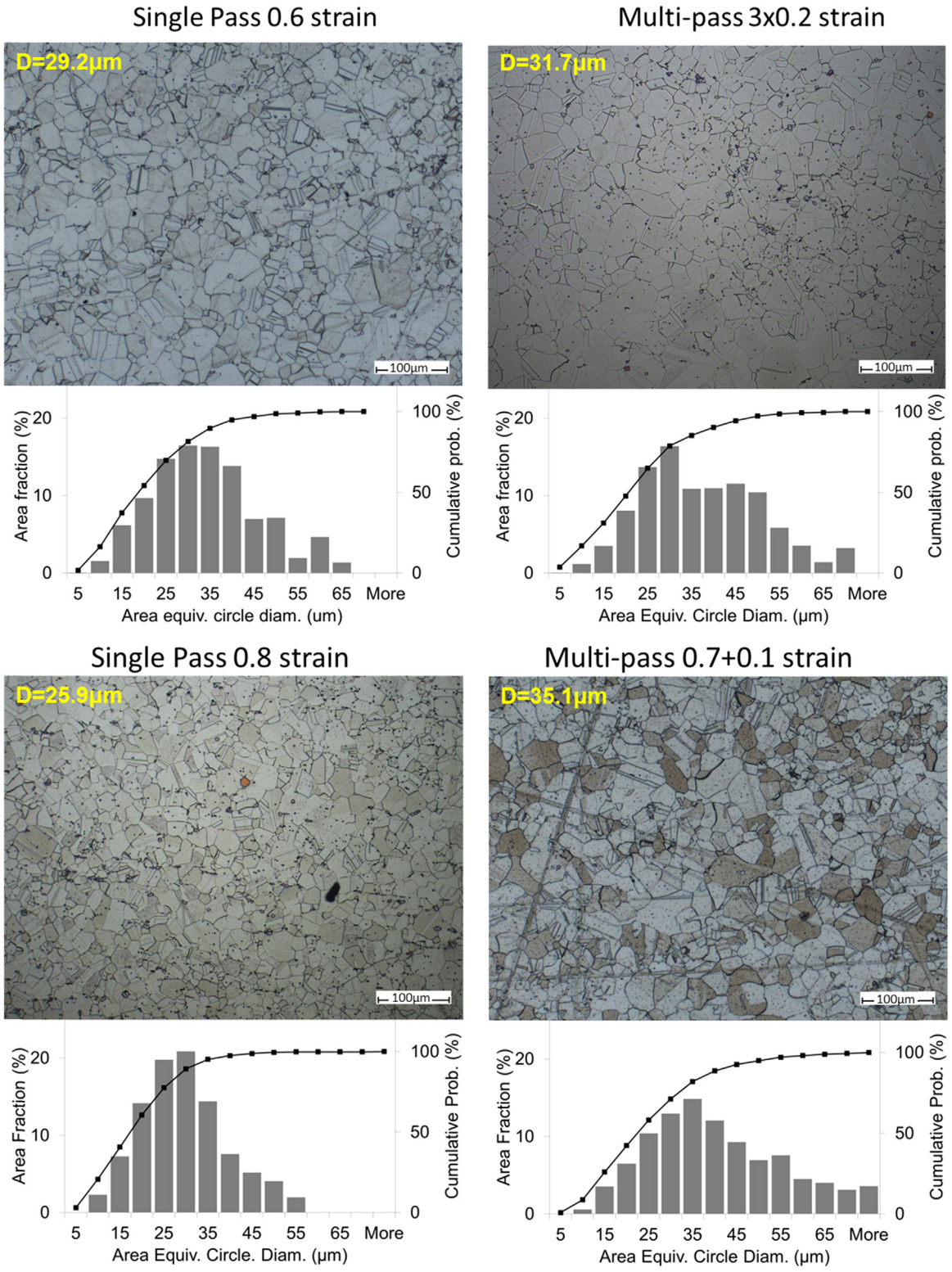

Fig. 8. Micrograph, grain size distribution, cumulative probability of diameter and mean feret grain size histogram for different strain conditions.

similar pattern to previous results showing an increase in flow stress initially. The critical strain for DRX is just surpassed in this 2nd pass so the material begins to soften very slightly.

Fig. 7 also shows the effect of increasing the inter-pass time to 3 h for 0.8 engineering strain interrupted tests. The increased inter-pass annealing time does not affect the appearance of the yield peaks. Increasing the inter-pass time appears to soften the flow stress curve slightly.

3.3. Microstructural analysis

The microstructures obtained after forging displayed in Fig. 8 vary depending on processing conditions. These micrographs confirm a fully recrystallized microstructure showing no elongation due to the forging process. The dark precipitates are believed to be stringers from the VIM/VAR process redistributed during the forging process. EDX analysis revealed high levels of Ti, Mo and Cr

present in these precipitates and previous work by Boehlert and Longanbach [18] has revealed them to be MC carbides.

Tests performed to 0.6 total engineering strain were designed to investigate a 3-stage ring rolling process. Single-pass compression produced a mean grain size of 29.2 μm and a standard deviation of 10.7. Under multistage (MS) conditions (3 × 0.2 engineering strain) the mean grain size and standard deviation rise to 31.7 μm and 12.3. Therefore the multi-pass specimen has a less homogenized microstructure. The 95% confidence intervals for the single-pass and multi-pass tests were 0.91 and 1.61 respectively.

Higher strain testing was designed to replicate a large deformation, such as upsetting, followed by a small deformation, such as rounding. Single pass tests to 0.8 engineering strain produced a grain size of 25.9 μm and a standard deviation of 9.5. Two-pass, 0.7+0.1 engineering strain, tests produced a grain size of 35.1 μm and a standard deviation of 12.8. The single-pass tests produced a finer more homogenized microstructure than multi-pass tests. The 95% confidence intervals for the single-pass and multi-pass tests were 0.73 and 1.29 respectively meaning that the difference in grain size is statistically significant. It's worth noting that due to the differing final geometry of the 0.6 and 0.8 tests it is likely that the deformed pancake shape of the high strain specimens radiated heat more effectively, resulting in a slightly faster cooling rate.

An internal misorientation statistic map is a plot of the degree of misorientation within a grain. It is assumed that a low level of misorientation within a grain represents a grain that has fully recrystallized whereas a higher internal misorientation deviation represents a grain that has some retained deformation and/or substructure and may be described as deformed or sub-structured. Fig. 9(a) and (b) show the level of internal misorientation within each grain for the 0.8 single pass and 0.7+0.1 multi-pass samples respectively, with low average internal misorientation represented by blue grains and high misorientation grains (up to 10°) represented by red grains. The maps confirm that both samples have a recrystallized structure since both microstructures have grains with relatively low internal misorientation. However it can clearly be seen that the multi-pass sample has on average grains with a much lower internal misorientation compared to the single pass. This can be more readily seen in Fig. 9(c) which plots the relative frequencies of grains according to their internal misorientation in degrees. The plot shows that the multi-pass sample has a higher frequency of lower internal misorientation grains ranging from 0.5° to 1.5°, whereas the single pass microstructure has fewer low internal misorientation grains of 0.5–1.5° but a higher relative frequency of grains having an internal misorientation of 1.5–3.0°.

The previous tests were repeated with the addition of a two-step ageing heat treatment to assess the effect on microstructure shown in Fig. 10. The microstructures appear to have more defined grain boundaries which are assumed to be caused by the etchant attacking the aged grain boundaries more heavily than the unaged. Both grain sizes were slightly reduced with the difference in mean grain size between single pass and multi-pass specimens to 0.6 total engineering strain being reduced to 1.2 μm. The ageing treatment shouldn't have effected grain size and the slightly finer grain size could be attributed the ageing treatment making the etch more effective and revealing slightly more grain boundaries. Ageing also had very little effect on the grain size of 0.8 total engineering strain specimens.

Fig. 11 shows a summary of both un-aged and aged grain sizes. Tests which exceeded 0.2 true strain either in a single pass or multi-pass show a very similar grain size, especially after ageing. The 0.7+0.1 test shows a slightly larger grain size due to grain growth occurring during the inter-pass anneal. Although the 0.1 test shows the largest grain size it is still finer than the starting microstructure meaning that some recrystallization has occurred.

4. Discussion

4.1. Interrupted flow stress curves

Recrystallization during inter-pass annealing typically results in flow softening upon reloading for most materials, including steel [7] and aluminium alloys [11]. Flow hardening upon reloading has been reported in nickel [8] and magnesium alloys [10]. The interrupted tests reached a true strain between 0.2 and 0.25. At this point the material is estimated to be 20% recrystallized through DRX. It is thought that full recrystallization through SRX and grain growth would have occurred during the inter-pass anneal. It is possible that the large amount of grain growth occurring during the 1 h inter-pass anneal would have restricted grain boundary sliding during the subsequent deformation. This would offset the reduction in yield stress caused by recrystallization. If these tests were performed at a slower strain rate and in non-isothermal conditions, to better replicate industrial conditions, it is likely the single pass test would display a slightly higher final flow stress due to the specimen cooling.

Previous investigations by Mataya [19] and later by Jaeger et al. [20] have reported the yield points are due to solute atoms pinning the previous dislocation structure, resulting in a sharp increase in flow stress. This stress is then released when the

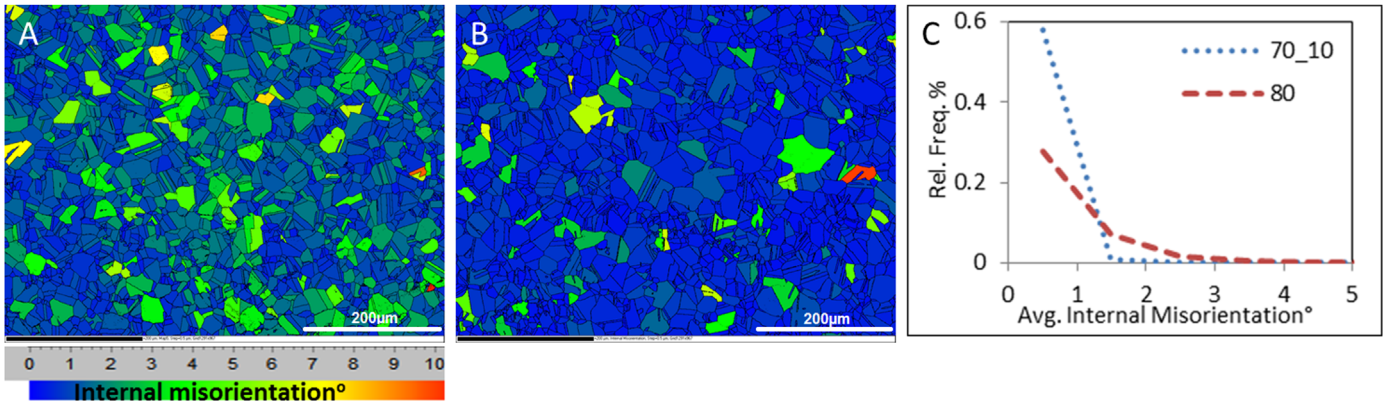

Fig. 9. EBSD Internal Misorientation map for (a) 0.8 Single pass and (b) 0.7+0.1 multi-pass and (c) histogram of the relative frequency vs average internal misorientation within each grain. (For interpretation of the references to color in this figure, the reader is referred to the web version of this article.)

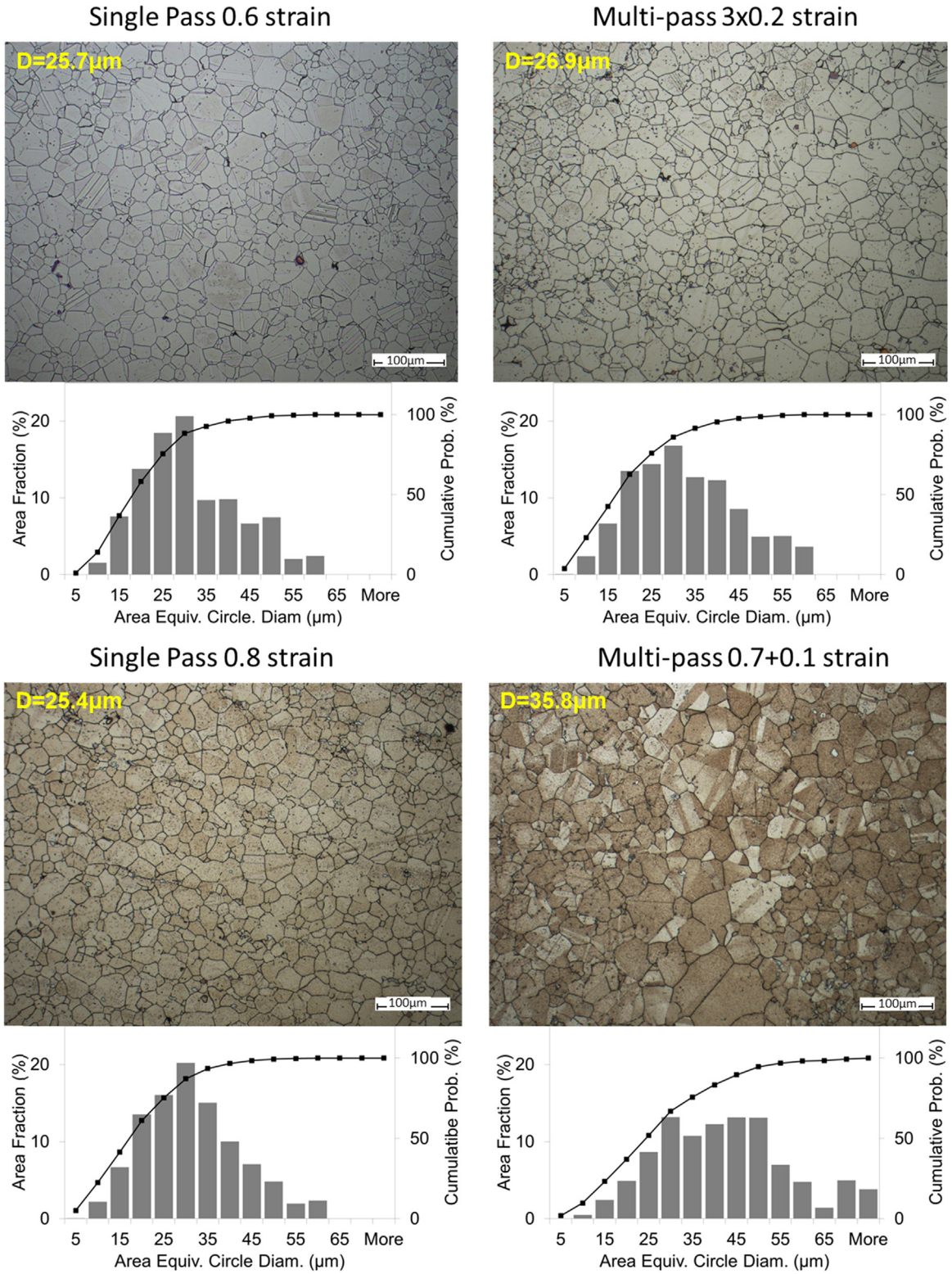

Fig. 10. Micrograph, grain size distribution, cumulative probability of diameter and mean feret grain size histogram for different strain conditions.

dislocations overcome these pinning elements. An investigation of the nickel superalloy Waspaloy noted these yield points were evident at 1100 °C due to being around the carbide solvus temperature [21]. However, previously reported yield points were evident in all deformation passes, whereas in the current investigation yield points were only evident in subsequent passes. Another possible explanation is due to friction effects, as during inter-pass times lubricant is burnt off, which increases friction for the second pass. As the material cannot slide against the die surface it becomes harder to deform, therefore raising stress. Once the stress reaches a peak level, the material slips, which rapidly reduces stress before it steadily increases again as the material work hardens. An additional test at 1150 °C was conducted to test this theory to see if there was a temperature dependence to this phenomenon. Fig. 6 shows the peaks were still visible at this higher temperature and when coupled with the lack of a yield

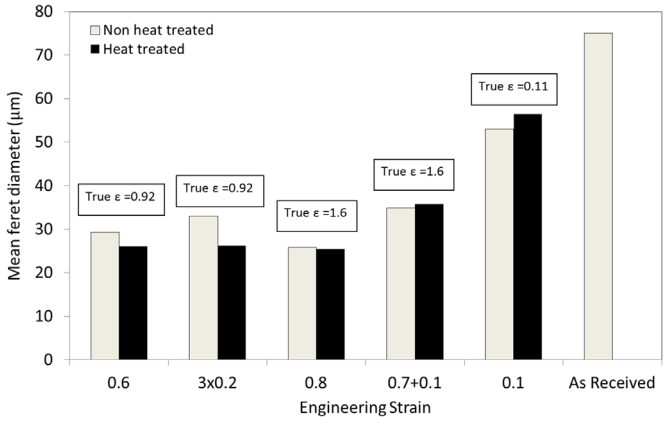

Fig. 11. Effect of heat treatment on feret grain diameter for different strain conditions.

peak on the first pass this suggests that excessive friction could be an alternative explanation for the presence of yield peaks. Further research would be required to test this theory.

4.2. Microstructural analysis

Forging to 0.8 total strain produced a fully recrystallized microstructure. This is partly due to DRX during forging above critical strains and partly due to static recrystallization after forging due to the lack of water quenching post forging, allowing further metadynamic recrystallization. It is known that Haynes 282 rapidly recrystallizes above critical strains through a combination of MDRX and SRX [12].

EBSD analysis revealed that both the single and multipass specimens were fully recrystallized due to the low levels of internal misorientation. However Fig. 9 clearly shows that the multipass sample has on average grains with a much lower internal misorientation compared to the single pass. It may be supposed then that both microstructures have undergone recrystallization however the single pass test retains some sub-structure. Once the steady state strain is reached during compression, DRX occurs continuously with little further effect on grain size. As this recrystallization is continuous the single pass microstructure is fully recrystallized but sub-structured. The multi-pass specimen would have had the same grain size as the single pass specimen after the first pass as both have surpassed the steady state strain determined in Fig. 2. During the inter-pass anneal significant grain growth occurred, resulting in a lower internal misorientation. The second pass introduced a small amount of DRX which bought the final grain size down slightly and resulted in a fully recrystallized final microstructure with low internal misorientation.

An additional single pass test to 0.1 engineering strain was completed in order to verify that DRX does occur during this second pass. The microstructure was partially recrystallized with a final grain size of 55 μm which is a reduction of 20 μm on the as-received grain size. This shows that the grain size was reduced during this second pass and also shows the extent to which the grain size must have grown during the inter-pass anneal. The recrystallization curve in Fig. 4 suggests that the material would not have fully recrystallized through DRX and it is possible further MDRX would occur after forging in the short time before the specimen was removed from the furnace.

For small strain increments the previous deformation step can be ignored when simulating multi-pass forging. The 0.2 engineering strain steps produced enough DRX to offset any grain growth occurring during the inter-pass anneal. The 0.1 engineering strain was just above the critical true strain of 0.09 required for DRX, however it did not produce enough DRX to bring down the grain size fully after an inter-pass anneal. As strains experienced during most forging processes such as ring rolling are well above the critical strain for DRX then only the final pass needs to be replicated in a laboratory environment.

5. Conclusions

- SRX plus grain growth during the inter-pass hold time produces a hardening effect, resulting in higher stress upon reloading. This is thought to be caused by the grain growth during the inter-pass anneal, hindering grain boundary sliding.
- Critical strain for DRX under these conditions is estimated to be 0.09 true strain.
- Another possible explanation for the presence of yield peaks could be due to the frictional effect of lubricant removal/burn-off during inter-pass annealing.
- The higher grain size observed for multi-pass specimens is due to grain growth occurring during the inter-pass anneal
- Prior forging history can effectively be ignored when replicating forging in a laboratory environment, provided the material experiences sufficient DRX in the final pass.

Acknowledgements

The current research was funded under the EPSRC Rolls-Royce Strategic Partnership in Structural Metallic Systems for Gas Turbines (grants EP/H500383/1 and EP/H022309/1). The provision of materials and supporting information from Rolls-Royce plc is gratefully acknowledged. Testing was performed at Swansea Materials Research and Testing Ltd. (SMaRT).

The authors would like to thank David Metzler at Haynes international for his material specific input and Doncasters Blaenavon for an insight into the ring rolling process.

References

[1] Gangshu Shen, David Furrer, Manufacturing of aerospace forgings, J. Mater. Process. Technol. (2000) 189–195.
[2] J.L. Song, A.L. Dowson, M.H. Jacobs, J. Brooks, I. Beden, Coupled thermo-mechanical finite-element modelling of hot ring rolling process, J. Mater. Process. Technol. (2002) 332–340.
[3] SFTC. ⟨www.deform.com⟩, 2014.
[4] Ding Hanlin, Hirai Kazuki, Homma Tomoyuki, Kamado Shigeharu, Numerical simulation for microstructure evolution in AM50 Mg alloy during, Comput. Mater. Sci. (2010) 919–925.
[5] Zhichao Sun, He Yang, Xinzhe Ou, Effects of process parameters on microstructural evolution during hot ring rolling, Comput. Mater. Sci. (2010) 134–142.
[6] Madlen Ullmanna, Grafa Marcel, Schmidtchena Matthias, Kawallaa Rudolf, Metadynamic recrystallization kinetics of twin roll cast AZ31 alloy during hot deformation, Procedia Eng. (2014).
[7] J. Liu, Y.G. Liu, H. Lin, M.Q. Li, The metadynamic recrystallization in the two-stage isothermal compression of 300M steel, Mater. Sci. Eng. A (2013).
[8] N.K. Park, I.S. Kim, Y.S. Na, J.T. Yeom, Hot forging of a nickel-base superalloy, J. Mater. Process. Technol. (2001).
[9] D.S. Weaver, S.L. Semiatin, Recrystallization and grain-growth behavior of a nickel-base superalloy during multi-hit deformation, Scr. Mater. (2007).
[10] M.H. Maghsoudi, A. Zarei-Hanzak, P. Changizian, A. Marandi, Metadynamic recrystallization behavior of AZ61 magnesium alloy, Mater. Des. (2014).
[11] Y.C. Lin, Lei.-Ting. Li, Yu.-Chi. Xia, A new method to predict the metadynamic recrystallization behavior in 2124 aluminum alloy, Comput. Mater. Sci. (2011).
[12] D. Metzler, M.G. Fahrmann, The effect of prior TMP on annealed grain size in Haynes 282 alloy, in: Proceedings of the 8th International Symposium on Superalloy 718 and Derivatives, TMS (The Minerals, Metals & Materials Society), 2014.
[13] HaynesIntl. HAYNES® 282® alloy product brouchure. ⟨www.haynesintl.com/pdf/h3173.pdf⟩, 2011.
[14] E407-07E1, ASTM. Standard practice for microetching Metals and Alloys. ASTM

international, 2007.
[15] C.A. Schneider, NIH Image to ImageJ: 25 years of image analysis, Nat. Methods (2012) 671–675.
[16] Y. Estrin, H. Mecking, A unified phenomenological description of work hardening and creep based on one-parameter models, Acta Mater. (1984).
[17] Xiao.-Min. Chen, Y.C. Lin, Dong.-Xu. Wen, Jin.-Long. Zhang, Min He, Dynamic recrystallization behavior of a typical nickel-based superalloy during hot deformation, Mater. Des. (2014).
[18] C.J. Boehlert, S.C. Longanbach, A comparison of the microstructure and creep behaviour of cold rolled HAYNES 230 alloy and HAYNES 282 alloy, Mater. Sci. Eng. A (2011).
[19] M.C. Mataya, Simulating microstructural evolution during the hot working of alloy 718, J. Miner. Met. Mater. Soc. (1991).
[20] J. Jaeger, D. Solas, T. Baudin, O. Fandeur, J.-H. Schmitt, C. Rey, Inconel 718 single and multipass modelling of hot forging, in: Proceedings of the 12th International Symposium on Superalloys, 2012.
[21] A.A. Guimaraes, J.J. Jonas, Recrystallization and aging effects associated with the high temperature deformation of waspaloy and inconel 718, Met. Trans. A (1981).